Morphology Studies of *trans*-1,4-Diisocyanatocyclohexane-Based Urethane Elastomers by Synchrotron X-ray Diffraction

C. Richard Desper* and Catherine A. Byrne

Polymer Research Branch, United States Army Research Laboratory, Materials Directorate, Watertown, Massachusetts 02172-0001

Yingjie Li and Benjamin Chu

Department of Chemistry, State University of New York at Stony Brook, Stony Brook, New York 11794-3400

Received November 7, 1994; Revised Manuscript Received February 26, 1995[⊗]

ABSTRACT: Urethane elastomers having hard segments based on CHDI [*trans*-1,4-diisocyanatocyclohexane] and BD [1,4-butanediol] are notable for their high softening temperatures and low hysteretic heat buildup. Experimental studies as a function of temperature using both wide- and small-angle X-ray diffraction of a series of such elastomers, incorporating PTMO [poly(tetramethylene oxide)] soft segments, reveal the persistence of hard-segment microdomains up to 275 °C. These hard-segment microdomains appear to be paracrystalline at ambient temperature, transforming to a glassy structure above ca. 100 °C. The glassy hard-segment structure is rigid to at least 275 °C, conferring rubbery properties on the material. Electron density variance data obtained by SAXS indicate that there is little hard- and soft-segment mixing at 30 °C for elastomers for which the molar ratio BD/PTMO is less than 2.0, with some segmental mixing indicated for higher BD/PTMO ratios. Changes in the microdomain structure with temperature are, for the most part, reversible for an elastomer with shorter hard segments corresponding to BD/PTMO = 1.5 but show marked irreversibility for one in which BD/PTMO = 3. These results are found to be consistent with models based on model compound data for the hard-segment packing.

Introduction

Urethane segmented copolymer elastomers prepared from *trans*-1,4-diisocyanatocyclohexane (CHDI) and 1,4-butanediol (BD) have been of interest[1] for their high tensile modulus and strength, high tear strength, high softening temperature, and excellent compressive fatigue behavior. In general, urethane elastomers owe their rubbery properties to microphase separation, involving the segregation of hard segments and soft segments into distinct microdomains[2–5] having size parameters in the range of 5–20 nm. For elastomers consisting of CHDI/BD hard segments and poly(tetramethylene oxide) (PTMO) soft segments, thermal analysis evidence has indicated the presence of ordered hard-segment microdomains, accounting for their superior thermal and mechanical properties.[1] These highly ordered hard-segment microdomains result, in turn, from the unusually compact symmetrical structure of the CHDI residue in the hard segment.

The hard-segment and soft-segment constituents of the polymer molecule are physically incompatible to their basic thermodynamic parameters, possessing a strong tendency to separate into two phases. However, because the two constituents comprise a block copolymer, with each sequence of a particular constituent being followed by a run of monomers of the other species, the phase separation, if it occurs, must occur at the submicroscopic level. In effect, the domain size of a microphase rich in one or the other molecular species is limited partially by the dimensions of the individual molecular blocks, confining domains to dimensions in the range of tens to hundreds of angstroms. The thermal and mechanical properties of such polyurethane elastomers have been studied in terms of this microphase separation model, with the details of the microstructure being elucidated by X-ray diffraction, DSC, and spectroscopic methods. Small-angle X-ray scattering (SAXS) has proven to be particularly useful[2–9] for studying the microphase separation in these materials.

A segmented urethane polymer is elastic for temperatures in which the soft-segment microphase is rubbery in character, while the hard-segment microphase is glassy or crystalline. Accordingly, such a polymer has as an upper bound of its elastomeric properties the temperature at which the hard-segment microphase loses its rigidity. This would be, as the case may be for the particular polymer, either the hard-segment glass transition temperature or its crystalline softening temperature. Crystallization, however, is not essential for elastomeric properties, provided that the hard-segment glass transition temperature is acceptably high. As an example, in the widely studied class of urethane elastomers whose hard segments are composed of 4,4′-diphenylmethanediisocyanate (MDI) and 1,4-butanediol (BD), elastomeric properties have been seen in conjunction with crystalline hard segments[9–13] or in conjunction with glassy, noncrystalline hard segments.[2,3,14] The question of whether a particular urethane in this class, or in any other class, will crystallize depends upon the details of the hard-segment composition and of the thermomechanical history of the polymer. For the MDI/BD class, hydrogen bonding between NH and carbonyl has been demonstrated by Bonart et al.[3] The energetics of this interaction provides an important contribution to the thermodynamic driving force related to the microphase separation process, favoring association of like chemical repeat units rather than mixing of dissimilar chemical repeat units. The structure of the hard-segment microphases may, in different instances, be glassy or show three-dimensional crystallinity or a structure of intermediate two-dimensional order.

The Bonart paracrystalline model[2,3] postulates a defective structure characterized by parallel ordering of hard-segment chains in two dimensions. The im-

[⊗] Abstract published in *Advance ACS Abstracts,* April 15, 1995.

0024-9297/95/2228-4213$09.00/0

proved opportunity for hydrogen-bonding interactions, compared to the glassy state, results in improved microphase separation and a higher temperature limit for elasticity. However, hydrogen bonding is not essential for elastomeric behavior in a polyurethane. Certain urethane elastomers containing hard segments composed of piperazine and 1,4-butanediol bischloroformate [Harrell[15] and Allegrezza et al.[16]], where the usual NH or OH to carbonyl hydrogen bonding is precluded by the lack of a hydrogen on the piperazine nitrogen atom, have shown elastomeric properties. Furthermore, recent theoretical molecular simulation work[17] suggests that entropic effects may contribute significantly to the free energy driving the microphase separation process. Thus, hydrogen bonding is not, by itself, essential to microphase separation.

The subject of the present work is the class of urethane elastomers in which the hard segment is the reaction product of *trans*-1,4-diisocyanatocyclohexane (CHDI) and 1,4-butanediol (BD). The thermal and mechanical properties of elastomers of this class have been reported by Siegmann et al.[18] and by Byrne et al.[19] The important characteristics of these elastomers, responsible for their continuing interest, is their high-temperature mechanical properties. As indicated by both Rheovibron and thermomechanical analysis, the elastomeric properties of elastomers in this class persist to temperatures well above those at which more conventional urethane elastomers, such as those of the MDI/BD class, give out. Both the Siegmann and the Byrne papers contain wide-angle X-ray diffraction data which show, in some instances, preliminary evidence of hard-segment crystallization, consisting of small crystalline peaks superimposed on a strong amorphous halo. One factor leading to difficulties in observing hard-segment crystallization in such patterns is the low weight fraction of the hard segment, around 20%, in typical elastomers of this class. Thus the hard-segment pattern must be observed as a small contribution in the presence of a strong soft-segment pattern from the 80% poly(tetramethylene oxide) (PTMO) in the formulations used by Siegmann and by Byrne. The latter is typically amorphous but can show soft-segment crystallinity when PTMO segmental molecular weights approaching 3000 are used.

The hard-segment structures of urethanes based on CHDI have also been studied by Jasinski[20] using the model compound approach involving the condensation products of CHDI with a monofunctional alcohol. Such compounds are white crystalline solids of quite high melting points: the dimethoxy compound melted at 270 °C, while the di-*n*-butoxy compound showed evidence of decomposition, but not of melting, in the 230–277 °C range. The computer modeling results of Jasinski,[20] based on single-crystal X-ray diffraction studies of such model compounds, show quite strong thermodynamic interactions on a theoretical basis, pointing to highly energetic interactions of the analogous hard-segment species, which are responsible for the high-temperature mechanical properties observed in this class of urethane elastomers.

Experimental Conditions

Urethane Elastomer Samples. Polymerization was accomplished by using a two-step, prepolymer method. The soft-segment oligomer, poly(tetramethylene oxide) (PTMO), was degassed by heating at 100 °C for 1 h with stirring and under vacuum, at which point the required amount of melted *trans*-1,4-diisocyanatocyclohexane (CHDI) was added all at once.

Table 1. CHDI Polyurethane Compositions

sample	molar composition CHDI	PTMO	BD	PTMO M_n	NCO/OH molar ratio	wt fract hard seg (M_H)
A	2.13	1.0	1.5	2030	0.85	0.188
B	2.25	1.0	1.5	2030	0.90	0.194
C	2.38	1.0	1.5	2030	0.95	0.200
D	2.50	1.0	1.5	2030	1.00	0.206
E	2.63	1.0	1.5	1930	1.05	0.221
F	2.75	1.0	1.5	1930	1.10	0.227
G	2.88	1.0	1.5	2030	1.15	0.224
H	3.00	1.0	1.5	2030	1.20	0.230
I	3.00	1.0	2.0	1930	1.00	0.252
J	4.00	1.0	3.0	1930	1.00	0.317
K	2.00	1.0	1.0	2860	1.00	0.122
L	4.00	1.0	3.0	2860	1.00	0.239
M	5.00	1.0	4.0	2860	1.00	0.286

This mixture was reacted, with stirring under nitrogen, for 1.5 h, or until a titration of the isocyanate group indicated its theoretical end-point value to within 0.3%. Next, the 1,4-butanediol (BD) chain extender, preheated to 100 °C, was mixed with the prepolymer rapidly for 1 min, at which point the mixture was degassed and poured into a mold with a cavity of dimensions 152.4 × 152.4 × 1.3 mm^3. The mold was transferred first to a hot press (100 °C, 100 psi, 1 h) and then removed from the press for an additional 15 h of cure in a 100 °C oven.

The polymer compositions are shown in Table 1. The polymers consisted of the following: (a) a series having a fixed BD/PTMO ratio of 1.5 and (approximately) fixed PTMO M_n of 2.0 × 10^3, while the NCO/OH ratio varies between 0.85 and 1.20 because of variation in the CHDI molar content; (b) a series having a fixed NCO/OH ratio of 1.00, with varied CHDI/PTMO ratios between 2.0 and 5.0, with PTMO M_n values of ca. 2.0 × 10^3 or 2.9 × 10^3. It was not possible to hold the PTMO M_n value strictly constant, since occasionally a given lot of PTMO would be exhausted. Although we shall designate a series of polymers as having a certain nominal PTMO M_n value, e.g., 2.0 × 10^3, the correct M_n for a specified polymer is used in calculations.

X-ray Diffraction Apparatus. Experimental X-ray diffraction data were obtained in both the small-angle and wide-angle ranges at the X3A2 beamline of the National Synchrotron Light Source (NSLS), located at the Brookhaven National Laboratory in Upton, NY. The experimental setup comprised (1) a primary beam collimation system,[21] (2) a sample heating cell, (3) a vacuum flight path, (4) and a Braun position-sensitive proportional counter interfaced via a Camac multiple channel analyzer (MCA) module to a Microvax II computer. Either wide- or small-angle diffraction patterns could be measured by positioning the detector at different distances from the sample. A heating chamber was used for varying sample temperature, which was held fixed to within 1 °C as each pattern was obtained. Between patterns, the temperature could be changed at an average rate of 15 °C/min. In all cases a wavelength of 0.154 nm (1.54 Å) was used.

The X-ray diffraction apparatus used in the synchrotron experiments included a modified Kratky block collimator in the primary beam collimation system[21] to reduce parasitic scattering. However, the beam length d was kept quite small to effectively eliminate the slit-length smearing effect. Thus the data were equivalent to data from "pinhole" collimation, in the sense that no desmearing correction was needed. For convenience, such data shall be referred to as pinhole optics data, even though the beam cross section was rectangular.

With regards to the synchrotron experiments, it must be noted that beamline stability is an issue to be taken into account. The primary beam intensity in the SAXS instrument is not constant because of decay, over a period of hours, in the synchrotron beam intensity and because of fluctuations in the position of the electron current ring vis-à-vis the instrument slits. Two ionization chambers were used to monitor the primary beam power in the SAXS instrument, one each before and after the sample position. Readings from both instruments were recorded at the start and end of each experimental pattern.

Additional small-angle X-ray scattering patterns were obtained using a Kratky camera fitted with a Technology for Energy Corporation position-sensitive proportional counter with a conventional X-ray generator at the U.S. Army Research Laboratory. This instrument does not provide desmeared data; rather it provides data representative of the infinite-slit-smeared case. The conventional SAXS instrument afforded a much wider angular range, to $q = 3.5$ nm^{-1} instead of 1.2 nm^{-1} for the Brookhaven instrument used for the SAXS work. Thus the Kratky camera data extend much further into the Porod tail region and are more suitable for accurate determination of values of the Porod invariant. The Kratky camera data are used only for determining such derived numerical quantities, where desmearing of the data is not required. No effort was made to desmear the Kratky camera data, since their only use was for calculating the electron density variance, for which an equation involving the infinite-slit-smeared intensity was available (see Bonart and Muller[4]).

Theoretical Treatment of SAXS Data

General Remarks. Treatment of the small-angle X-ray scattering data follows, in general terms, previously established methods.[7] However, for the sake of clarity, it was found useful to deal comprehensively with the equations used, relating the concepts systematically and introducing a new concept, the "reduced intensity".

All SAXS patterns are reported with respect to the variable $q \equiv h \equiv (4\pi/\lambda) \sin\theta$, where λ is the wavelength (0.154 nm in this work) and 2θ is the scattering angle.

Average Squared Electron Density Fluctuation. The determination from SAXS data of the average squared electron density fluctuation, $\langle\Delta\varrho_e^2\rangle'$, which may be referred to as the electron density variance, has been described by Kratky.[22] The single prime in $\langle\Delta\varrho_e^2\rangle'$ follows the convention of Bonart and Muller[4] and of Koberstein and Stein[23] to indicate that the data have been corrected for background and diffuse scattering but not for nonzero interface thickness which gives departure from Porod's law in the tail region. The method may be used with either desmeared or infinite-slit-smeared intensity data and requires an appropriate integration over such data. In addition, a method for the determination of the power of the SAXS primary beam is required in order to place the data in absolute rather than relative terms. For infinite-slit-smeared data, e.g., when a Kratky camera is used to collect data, a standard sample of Lupolen polyethylene calibrated in Dr. Kratky's laboratory[24] may be used to determine the power of the beam. Different standard samples may be more appropriate for a pinhole optics instrument which yields desmeared data directly, such as those commonly used with synchrotron radiation. Appropriate standard samples in this case have been discussed by Russell.[25]

Using desmeared data, the electron density variance $\langle\Delta\varrho_e^2\rangle'$ may be determined (following Kratky[22]) from:

$$\langle\Delta\varrho_e^2\rangle' = (C_k D a P_s)^{-1}(a\lambda/2\pi)^3 \int_0^{+\infty} q^2 I(q)\, dq \quad (1)$$

where the quantities involved are defined in Tables 2 and 3. For infinite-slit-smeared data, the electron density variance is obtained instead from:

$$\langle\Delta\varrho_e^2\rangle' = (2C_k D a P_s)^{-1}(a\lambda/2\pi)^2 \int_0^{+\infty} q\tilde{I}(q)\, dq \quad (2)$$

Extrapolation to Zero and Infinity for Porod Invariant Determination. Whether the data is desmeared or infinite-slit-smeared, however, the integration required to determine the electron density variance has q limits from zero to infinity. Because of obvious instrumental limitations, the experimental data will not extend to either end point but will be limited to a range $q_L \le q \le q_H$. Thus methods may be needed to extrapolate the intensity curves in the low end range $0 \le q \le q_L$ and the high end range $q_H \le q < \infty$. For the low end a Guinier law (Gaussian) function is used if needed, i.e., if the intensity is rising as q descends into the extrapolation range. For the high end, either Porod's law:

$$I(q) = K_p q^{-n} \quad (3)$$

where K_p is a parameter characteristic of the sample and n is 4 for desmeared and 3 for infinite slit data, or an empirical equation, where the power n is replaced by an empirically determined floating point number, may be used. Once the curve fit parameters are established at either end, the extrapolation contribution to the required integral may be calculated from an analytical expression. In practice, it is preferable that the extrapolation parts of the integral be small compared to the experimental part of the integral. In the present work, the extrapolation to zero angle was omitted for both infinite slit or pinhole collimation data, while the extrapolation to infinite angle was used for the infinite-slit-smeared data only. The electron density variance values from the synchrotron data should be used for comparative purposes only; the results from the infinite slit instrument are more accurate. Because of the very wide range available using the Kratky instrument, the extrapolation to infinite angle could be applied at a larger q value, where it had a smaller influence on the total integration for the Porod invariant.

Table 2. Definition of Terms for Small-Angle X-ray Scattering

λ	X-ray wavelength, nm or Å at the discretion of the user
2θ	scattering angle, rad, for an individual intensity datum
a	sample-to-detector distance, cm
A_s	attenuation ratio for the sample, dimensionless
C_k	physical constant involving Avogadro's number and the Thomson scattering constant for an electron having the value 8.34×10^{-3} cm^3/mol^2; from Kratky[22]
D	sample thickness, cm
$I(q)$	intensity measured at the indicated value of the scattering variable q, using pinhole optics
$\tilde{I}(q)$	intensity measured at the indicated value of the scattering variable q, using slit optics
P_0	primary beam power incident on the sample
P_s	primary beam power as attenuated by the sample
P_{std}	power (incident on the sample) of a hypothetical standard primary beam of constant intensity
q	scattering variable $(4\pi/\lambda) \sin\theta$, units are inverse of the units of λ
ϱ_e	electron density, mol e/cm^3; its fluctuation in space gives rise to X-ray scattering

Definition of Absolute SAXS Scattered Intensity $I_{abs}(q)$. There are two different approaches to defining scattered SAXS intensities in absolute terms, namely, that of Kratky,[22] where the scattered intensity $I(q)$ is divided by P_s, as in eqs 1 and 2, and that of Russell et al.,[25] in which an absolute differential scattering cross section per unit volume $d\Sigma(q)/d\Omega$ is used. Since the formalism of the two approaches differs, although each is valid in its own context, it is necessary to select one or the other to continue. The Kratky approach has been selected, largely on the basis that its formalism deals with both desmeared and infinite-slit-smeared data. An absolute scattered intensity function $I_{abs}(q)$ is defined as:

Table 3. Definitions for Electron Density Variance Calculations

symbol	units	definition
$\langle\Delta\varrho_e^2\rangle$	$(\text{mol e/cm}^3)^2$	variance (mean-squared variation from the average value) of the electron density: with no corrections applied, this represents the variance of a real system with diffuse domain boundaries and statistical density fluctuations within the microphases, as in Figure 4c of Bonart and Muller[4]
$\langle\Delta\varrho_e^2\rangle'$	$(\text{mol e/cm}^3)^2$	electron density variance value of a system corrected for fluctuations within the microphases, but not for diffuse microphase boundaries, as in Figure 4b of Bonart and Muller[4]
$\langle\Delta\varrho_e^2\rangle''$	$(\text{mol e/cm}^3)^2$	electron density variance value of a system corrected for both fluctuations within the microphases and for diffuse microphase boundaries, as in Figure 4a of Bonart and Muller[4]
$\langle\Delta\varrho_e^2\rangle_P$	$(\text{mol e/cm}^3)^2$	electron density variance value of a fully microphase-separated system[a]
M_H	g/cm^3	mass fraction of hard-segment species
M_S	g/cm^3	mass fraction of soft-segment species
R_H	mol e/g	for hard segment: conversion factor[b] from mass density to electron density
R_S	mol e/g	for soft segment: conversion factor[b] from mass density to electron density
ϕ_H	dimensionless	volume fraction of hard-segment microphase
ϕ_{HP}	dimensionless	volume fraction of hard-segment microphase of a fully separated system[a]
ϕ_S	dimensionless	volume fraction of soft-segment microphase
ϕ_{SP}	dimensionless	volume fraction of soft-segment microphase of a fully separated system[a]
μ_H	g/cm^3	mass density of hard-segment microphase
μ_{HP}	g/cm^3	mass density of hard-segment microphase of a fully separated system[a]
μ_S	g/cm^3	mass density of soft-segment microphase
μ_{SP}	g/cm^3	mass density of soft-segment microphase of a fully separated system[a]
ϱ_H	mol e/cm^3	electron density of hard-segment microphase
ϱ_{HP}	mol e/cm^3	electron density of hard-segment microphase of a fully separated system[a]
ϱ_S	mol e/cm^3	electron density of soft-segment microphase
ϱ_{SP}	mol e/cm^3	electron density of soft-segment microphase of a fully separated system[a]

[a] A fully microphase-separated system is an idealized system consisting of pure hard- and soft-segment microphases with sharp microphase boundaries. [b] Such conversion factors are simply the ratios of the total atomic number to the total atomic weight for the species in question.

$$I_{abs}(q) \equiv (I(q)\, a^2)/(P_0 D A_s) \tag{4}$$

for desmeared data and as $\tilde{I}_{abs}(q)$ for infinite-slit-smeared data:

$$\tilde{I}_{abs}(q) \equiv (\tilde{I}(q)\, a^1)/(P_0 D A_s) \tag{5}$$

These functions compensate for the instrumental parameters P_0 and a^p, and the sample parameters D and A_s, yielding a scattering curve characteristic of the sample morphology in both shape and magnitude. The value of the exponent of a in each case reflects the dimensionality of the experimental setup. The primary beam power P_0 incident on the sample is related to its power P_s as transmitted through the sample by:

$$P_s = P_0 A_s \tag{6}$$

Koberstein and Stein[23] have defined a "Rayleigh ratio" $R(h)$ in analogy with light scattering terminology. Comparing $R(h)$ as defined in their eq 3 with $I_{abs}(q)$ defined in eq 4, the only difference, noting that h and q are equivalent, is that Koberstein and Stein incorporate the sample absorption A_s into their definition of beam power. In the present work, both desmeared and infinite-slit-smeared data may be dealt with conveniently with a single computer program, provided one accounts properly for the dimensionality of the experiment, which is 2 for the desmeared (synchrotron) instrument vs 1 for the infinite-slit-smeared (Kratky) instrument.

Primary Beam Power Calibration. We shall deal with absolute intensities only in the context of the Kratky camera data. In the case of infinite-slit-smeared (Kratky) data, the primary beam power is determined by the method of Kratky,[24] using the intensity $\tilde{I}_{c,150}$ from the Lupolen standard measured at an angle corresponding to a Bragg d spacing of 150 Å. The primary beam intensity P_s may be calculated from:

$$P_s = C_{Lupolen} A_s a_{Lup} \tilde{I}_{c,150} \tag{7}$$

using the value of the value of the constant $C_{Lupolen}$ provided with the calibration sample. In eq 7, a_{Lup} is the value of the distance a at which the Lupolen calibration is performed. This value is usually unchanged when other data sets are measured, but for generality, we shall distinguish between the two.

Definition of the Reduced Intensity Function. Even if one should lack a means of absolute intensity calibration, a method for rendering the data into a form suitable for making useful comparisons between data sets on a relative basis has been devised and put into effect. For this purpose, let us introduce here a reduced intensity $I_{red}(q)$, defined as:

$$I_{red}(q) = I(q)[a^2/(DA_s)] \tag{8}$$

for desmeared data and

$$\tilde{I}_{red}(q) = \tilde{I}(q)[a^1/(DA_s)] \tag{9}$$

for infinite slit-smeared data. Comparing with eqs 4 and 5, the reduced intensity function contains compensation for the instrument and specimen parameters a, D, and A_s, lacking only the P_0 divisor when compared with the absolute intensity function. The reduced intensity may be used in place of the absolute intensity for purposes of comparisons on a given instrument, including Porod invariant comparisons, as long as the results are recognized as relative values within a particular set of data, rather than as absolute values.

Compensation for Beam Power Decay. In experiments using the synchrotron radiation source, the decay of the beam power P_0 was monitored by use of an ionization chamber and the data sets were compensated accordingly. This method is of limited precision, however. Because of the limited precision of the readout device and the fact that beam power history was not followed continuously throughout the run, an imprecision estimated at 10% may remain in the measured

intensity levels and thus in quantities, such as the electron density variance values, dependent upon such intensity levels. Such data are deemed to be only semiquantitative and are not used for quantitative interpretations.

Diffusion Scattering Correction. In all of the aforementioned treatments of the SAXS data, one must correct for diffuse scattering arising from thermal motions and static disorder of the atoms within microdomains before proceeding further with calculations. The method used to determine the diffuse scattering intensity, proposed by Ruland,[26] consists of plotting $q^n I(q)$ versus q^n, where, as in eq 3, n assumes a value of 3 for infinite-slit-smeared data and 4 for desmeared data. In the Porod tail region, such a plot should follow a straight line with a negative slope; the absolute value of that slope is the diffuse scattering intensity.

Interface Thickness. Depending upon the nature of the material, the boundaries between microphases may not be sharp but may be characterized instead by a boundary layer of finite (nonzero) thickness. Such an interface boundary can lead to departure from Porod's law (eq 3), which would otherwise apply in the tail region for a system having sharp boundaries. The determination of the value of such an interface boundary thickness can be fraught with difficulties in terms of evaluating the proper correction to apply for diffuse scattering intensity. Such determinations have been discussed extensively[26-28] and will not be detailed here. Interface thicknesses were determined in the present work only for the infinite-slit data, using the method of Koberstein, Morra, and Stein.[27] In this method, the quantity $\ln(\tilde{I}(q)\ q^3)$ is plotted against $q^{1.81}$. At higher angles, this plot should become linear with a negative slope, and the interface thickness is calculated from the magnitude of that slope. Note that a system of sharp interface boundaries will show zero slope, while a positive slope indicates that not all of the diffuse scattering intensity has been subtracted.

Quantitative Interpretation of Electron Density Variance. In the simplest case, in which a material consists of two microphases of electron densities ϱ_H and ϱ_S, and corresponding volume fractions ϕ_H and ϕ_S, respectively, but NO diffuse boundary layer, the electron density variance $\langle \Delta\varrho_e^2 \rangle'$ may be written as:

$$\langle (\Delta\varrho_e)^2 \rangle' = \phi_H \phi_S (\varrho_H - \varrho_S)^2 = \phi_H (1 - \phi_H)(\varrho_H - \varrho_S)^2 \quad (10)$$

where the quantities involved are defined in Table 3. The experimental value for $\langle \Delta\varrho_e^2 \rangle'$ is obtained using eq 1 or eq 2, as applicable, for the short-slit-length (synchrotron) or the infinite-slit-length (Kratky camera) instrument.

In the case of diffuse boundaries, two approaches have been used. In the first approach, one may modify the Porod invariant equation to correct the experimental intensity before the indicated integration is performed. Thus Bonart and Muller[4] offer a modified form of eq 1 (their eq 21), dividing by a damping factor function obtained from the tail region fit for the interface thickness determination. The resulting equation yields directly a density variance value $\langle \Delta\varrho_e^2 \rangle''$ for an idealized system in which the boundaries are sharp. Note that a double prime is used, following Bonart and Muller,[4] to indicate that the value has been corrected for both diffuse scattering and diffuse microphase boundaries. For the case of the infinite-slit instrument, Leung and Koberstein[29] offer an analogous equation, their eq 6, in place of the present eq 2, which again yields directly the value of $\langle \Delta\varrho_e^2 \rangle''$.

Alternately, one may integrate first and then correct the experimental $\langle \Delta\varrho_e^2 \rangle'$ value as given from eq 1 or eq 2 for the effect of diffuse microphase boundaries to calculate $\langle \Delta\varrho_e^2 \rangle''$. Again, this requires an experimental interface thickness value from the tail region fit. An appropriate equation for this purpose is Desper and Schneider's[7] eq 16.

For the present urethane elastomers, the correction for a diffuse boundary was found to be unnecessary, as will be demonstrated. The actual boundary layer thicknesses are sufficiently small that they cannot be distinguished experimentally from zero thickness. Consequently, the data were analyzed by ignoring any effect of the diffuse boundary layer, in effect equating $\langle \Delta\varrho_e^2 \rangle'$ with $\langle \Delta\varrho_e^2 \rangle''$.

Inhomogeneity Length (Correlation Distance). The inhomogeneity length or correlation distance L_C, first defined by Porod,[7] is a reciprocally averaged length of vectors which span a section of a low-density microphase, followed by a section of a high-density microphase. Such a quantity may be determined[7] from the ratio of two integrals over all possible values of q:

$$L_C = \pi \int_0^{+\infty} qI(q)\, dq / \int_0^{+\infty} q^2 I(q)\, dq \quad (11)$$

for desmeared (pinhole optics) data and

$$L_C = 2 \int_0^{+\infty} \tilde{I}(q)\, dq / \int_0^{+\infty} q\tilde{I}(q)\, dq \quad (12)$$

for infinite-slit-smeared data. (Note that the constants 2 and π appearing in eqs 11 and 12 reflect the choice of q as the independent variable.) One may define L_H and L_S to be the inhomogeneity lengths in the hard- or soft-segment microphases, respectively. If one has knowledge of ϕ_H and ϕ_S, one may calculate L_H and L_S from:

$$L_H = L_C/(1 - \phi_H) \quad \text{and} \quad L_S = L_C/(1 - \phi_S) \quad (13)$$

Since the ratio of two integrals is involved, any calibration constants would cancel out, so the intensities involved in the integrations need not be in absolute terms. As for the electron density variance determination, however, some provision may be required to deal with those intensities which are experimentally inaccessible at the low and high ends of the integrations.

Computer Software. One of the present authors (C.R.D.) has written extensive computer software in the Fortran 77 language which was used in processing the data. This software, named MCAMENU, supports all of the corrections and calculations referred to herein and is particularly convenient for use in applications such as the present heating experiments, where multiple scans, generating multiple data files, are run for a single specimen. The software is user-friendly, menu-driven, supports graphics, and has built-in safeguards to keep track of which corrections have been applied to a particular data file. MCAMENU will be reported separately.

Experimental Results

Morphology Changes with Temperature As Studied by Wide-Angle X-ray Scattering. For CHDI/PTMO/BD polymers studied here the wide-angle X-ray scattering (WAXS) pattern, though definitely noncrystalline, showed subtle changes as a function of temperature. Three WAXS heating experiments were run

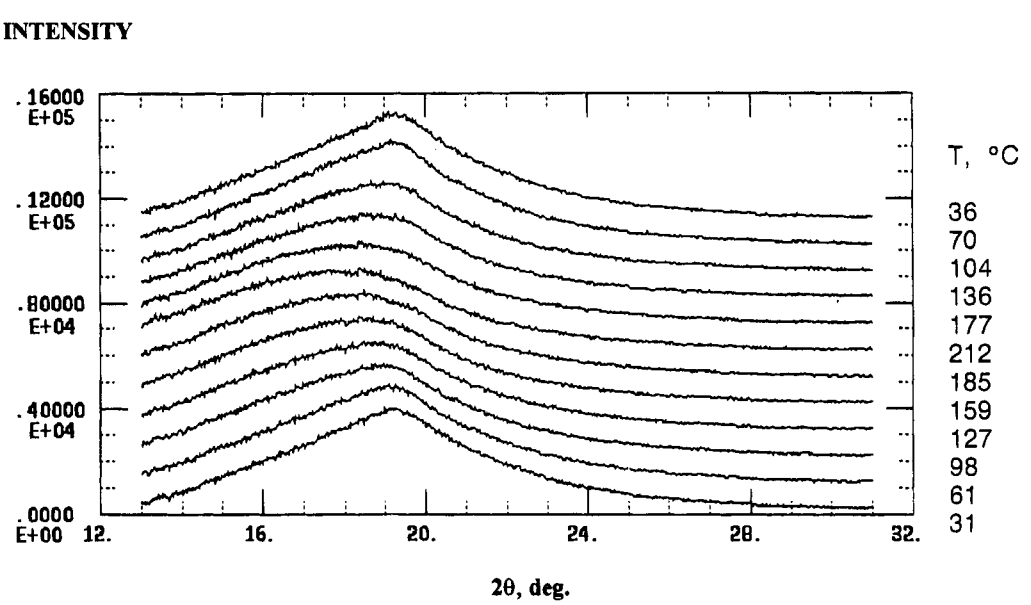

Figure 1. WAXS heating experiment (intensity vs 2θ, degrees) of polyurethane D from Table 1. Temperatures are indicated along the right vertical axis. Scans at intermediate temperatures are omitted, and successive plots are offset by an upward baseline shift.

using synchrotron radiation at temperatures beginning at ca. 30 °C, up to a high value of ca. 210 °C, and returning to ca. 30 °C, using compositions C, D, and H of Table 1. A set of patterns corresponding to composition D is show in Figure 1; patterns at the other two compositions were comparable. The temperature range was selected because of an exotherm in the DSC pattern around 185 °C, originally attributed to hard-segment crystallization. The premise of the heating experiment was to improve hard-segment order by passing through this transition at a slow rate. However, neither the first nor the last patterns, measured near room temperature, showed the multiple sharp peaks typical of crystalline material. On the other hand, the single maximum seen in the room temperature patterns near $2\theta = 19.3°$ (corresponding to a d spacing of 0.46 nm) was unusually more pointed in shape when compared with the rounded amorphous halo seen in the same range at elevated temperatures. The latter, exemplified by the pattern at 212 °C, is a typical amorphous polymer peak.

In general, the WAXS patterns obtained near room temperature have a sharpness at the top of the peak which, although not as sharp as the usual crystalline peaks, is noticeably different from the rounded amorphous peak seen at elevated temperatures in these experiments, or seen, in general, for amorphous polymers. The sharpness of the peak observed at lower temperatures is suggested to consist of a single fairly sharp peak originating from paracrystalline hard-segment material, superimposed on a rounded amorphous peak. Paracrystalline ordering is suggested in that the degree of lateral ordering is evidently higher than that of amorphous polymers but lower than that of semicrystalline polymers. An examination of the patterns obtained at various temperatures in Figure 1, as well as others not shown for the sake of brevity, obtained at additional intermediate temperatures, reveals that the sharpening of the peak persists from 30 °C up to around 100 °C with ascending temperature and then reappears again at ca. 100 °C as the temperature is lowered. Thus the disappearance of the structure responsible for the sharpened peak is definitely reversible. The temperature of disappearance and reappearance of the sharpened peak is always higher than any possible soft-segment transitions, so the peak could be associated with the hard-segment microphase. The only other published WAXS data for CHDI/BD hard-segment polyurethanes, that of Siegmann et al.,[18] showed the same sharpened peak seen here in their Figure 5c. The Siegmann elastomer consisted of CHDI and BD forming the hard segment, with HTPB (hydroxy-terminated polybutadiene) as the soft segment. The fact that the hard-segment composition is common to both studies, while the soft segment is not, strengthens the assignment of the sharpened peak to the hard-segment microphase.

Table 4. SAXS Interfacial Thickness Determinations from Slopes of Appropriate[a] Plots of Infinite-Slit-Smeared Data: CHDI-Based Elastomer Samples

sample	Koberstein slope,[b] $nm^{-1.81}$	interfacial thickness σ,[b] nm
A	0.0003	NA[c]
B	−0.0004	0.01
C	0.00008	NA[c]
D	−0.0006	0.01
E	−0.0007	0.02
F	0.0043	NA[c]
G	−0.0029	0.03
H	−0.0071	0.05
I	−0.0015	0.02
J	−0.045	0.15
K	−0.0009	0.02
L	−0.014	0.08
M	−0.045	0.15

[a] See Koberstein et al.[27] [b] Thickness determinations from curve fit range of $q^{1.81} = 2.30-3.25$ $nm^{-1.81}$, corresponding to $q = 1.6-1.9$ nm^{-1}. [c] N/A: a positive slope will not yield a thickness value.

Interpretation of Interface Thickness Values. The results of interface thickness σ determinations by SAXS, from the Kratky camera data at 30 °C, are shown in Table 4. The appropriate (Koberstein et al.)[27] plots (not shown) of $\ln(Iq^3)$ vs $q^{1.81}$ for all of the CHDI polyurethanes are quite close to horizontal for a long range of q values in the tail region, indicating interface thicknesses near zero, as shown in Table 4.

The assumption that the Kratky instrument is acting as an infinite-slit device was checked by a computer calculation based on Kratky, Porod, and Skala,[30] using

Table 5. SAXS Results on Lupolen Calibration Sample

data set no.	Koberstein slope,[a] $nm^{-1.81}$	interfacial thickness σ, nm	$\langle\Delta\varrho_e^2\rangle \times 10^3$,[b] (mol e/$cm^3$)^2
1	-0.55_2	0.61	1.48_3
2	-0.53_7	0.60	1.46_3
3	-0.49_1	0.57	1.48_6

[a] Curve fit range: from $q^{1.81} = 0.80-1.09$ $nm^{-1.81}$, corresponding to $q = 0.88-1.05$ nm^{-1}. [b] Experimental electron density variance value.

the values for the camera parameters in effect in these experiments. For the slit-collimated Kratky instrument, there is a limiting q, dependent upon slit optics parameters, above which the infinite-slit assumption does not hold.[31] Also, Ruland,[32] along with Koberstein and Stein,[23] have noted that data analysis for the purpose of determining the interface thickness should be limited to data at q values above any potential second-order maximum. These rules were both observed in the present determinations.

To verify the interface thickness determination method, three data sets from the Lupolen standard polyethylene sample were also analyzed in this manner. The results (Table 5) show interface thickness (σ) values of approximately 0.6 nm, quite appropriate for such polyethylenes and indicating that the near-zero σ values determined for these polyurethanes are not an artifact.

In any event, when an interface thickness value is less than or equal to the value of a typical chemical bond in the material, the most that can be said is that the σ value is experimentally indistinguishable from zero. Thus, considering that a carbon–carbon single bond has a bond length of 0.154 nm, no σ value of 0.154 nm or smaller may be considered significantly different from zero. Essentially, the premise of any interface thickness determination method is that the effect of interface thickness upon the SAXS tail region behavior may be separated from any effects of scattering resulting from interferences between individual atoms, such as diffuse scattering arising from atomic disorder effects. When the apparent interface thickness value is of the same scale as that of interatomic interferences, the assumption that small-angle scattering intensity may be mathematically separated from the diffuse scattering intensity no longer applies.

In summary, we may say that the polyurethane interfaces are deemed to be quite sharp in these samples. This is consistent with the soft-segment T_g data previously reported[19] for these elastomers, which are quite close to the T_g of the pure soft-segment phase, indicating that segmental mixing is minimal. However, it is not possible to state precisely how sharp the interfaces are, since the limit of the method, namely, the length of a covalent bond, has been approached by the values indicated in the experiment.

Microphase Separation As Studied by SAXS: Effect of Composition at 30 °C. Figure 2 shows the SAXS pattern at 30 °C of a series of seven polyurethanes of molar ratio BD/PTMO fixed at 1.5, but with the moles of CHDI varied in order to vary the total NCO/OH ratio from 0.85 to 1.15. The SAXS intensity is quite strong, indicative of a well-developed microphase separation morphology. The maximum in the pattern at $q \equiv (4\pi/\lambda)\sin\theta = 0.35$ nm^{-1} translates as a repeat period of $d \equiv 2\pi/q = 18.0$ nm. However, it must be recognized that the meaning of such a d spacing value from SAXS data can be somewhat ambiguous, even when a distinct peak is noted. If the maximum in the scattering curve is very broad, as it is for many of these curves, the concept of a repeat period may not necessarily apply. Nothing has been established as to the morphology underlying such a repeat period. Instead, one should view such d spacing numbers as mental guidelines indicating in general terms the size range at which inhomogeneity correlations occur.

The patterns at 30 °C for a series with molar composition CHDI:PTMO:BD = N:1:(N − 1), with the PTMO nominal molecular weight at 2000, are shown in Figure 3. As in Figure 2, the scattering maximum is at the same approximate position $q = 0.35$ nm^{-1}. These data indicate that the general size of microstructure elements is largely insensitive to the hard-segment sequence length or to the NCO/OH ratio, which is understandable in view of the relatively small weight fractions of the hard segment involved, as shown in Table 1. Figure 4, showing SAXS patterns at this temperature for a series of polymers containing longer (M_n = 2900) soft-segment lengths, shows a slightly shifted peak position at $q = 0.32$ nm^{-1}, corresponding to $d = 19.6$ nm. The SAXS maxima are quite broad for a number of polymers in Figures 2–4, rendering serious interpretation in terms of a repeating structure pointless.

Referring to Figures 2–4, however, it is evident that there is a great deal of variability in the strength of the SAXS peak, which is best studied quantitatively through the electron density variance values, obtained by the Porod invariant method.

The experimental electron density variances for the 13 elastomers, obtained at 30 °C, are shown in the second column of Table 6. These data were first tested against the simplest possible model, that of two microphases, each containing pure hard- and soft-segment species, and with no diffuse boundary layer. For this case eq 10 is modified by replacing the electron densities ϱ_H and ϱ_S with the pure microphase values ϱ_{HP} and ϱ_{SP} and the volume fractions ϕ_H and ϕ_S with the pure microphase values ϕ_{HP} and ϕ_{SP}:

$$\langle\Delta\varrho_e^2\rangle_P = \phi_{HP}\phi_{SP}(\varrho_{HP} - \varrho_{SP})^2 = \phi_{HP}(1 - \phi_{HP})(\varrho_{HP} - \varrho_{SP})^2 \quad (14)$$

The soft-segment mass and electron densities μ_{SP} and ϱ_{SP} are known[4] from studies of other PTMO-containing polyurethanes, but the hard-segment mass and electron densities are not known for the present class. However, for the purpose of testing against this simple model, sufficient information is available to calculate from eq 14, knowing the chemical compositions of the elastomers, the apparent electron density difference ($\varrho_{HP} - \varrho_{SP}$), assuming $\langle\Delta\varrho_e^2\rangle_P$ may be identified with the experimental variance value $\langle\Delta\varrho_e^2\rangle'$. Since ϱ_{SP} is known for the PTMO soft segment, one may then obtain the hard-segment electron density ϱ_{HP} and then the mass density μ_{HP}.

However, there is a minor complication which prevents using a direct solution for ϱ_{HP}: the composition data give us the mass fractions M_H and M_S, while eq 10 requires volume fractions. Calculation of the volume fractions requires knowledge of the microphase mass densities μ_{HP} and μ_{SP}, which in turn are proportional to the electron densities ϱ_{HP} and ϱ_{SP}, whose difference is sought. Thus the solution for $\varrho_{HP} - \varrho_{SP}$ is implicit rather than explicit, involving a small number of rather simple equations[7] which need not be repeated here. An iterative solution is readily obtained as outlined previously.[7] A Fortran computer program has been written

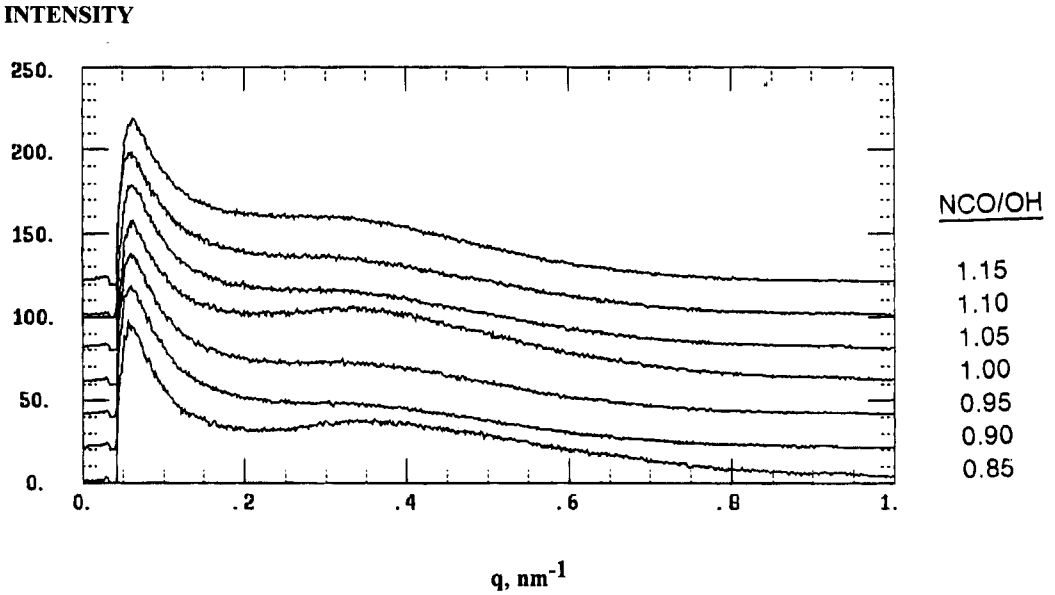

Figure 2. SAXS patterns (intensity vs q, nm^{-1}) of polyurethanes A–G (reading from the bottom curve upward) of Table 1, having NCO/OH ratios from 0.85 to 1.15. The PTMO has a nominal M_n of 2000. Successive plots are offset by an upward baseline shift.

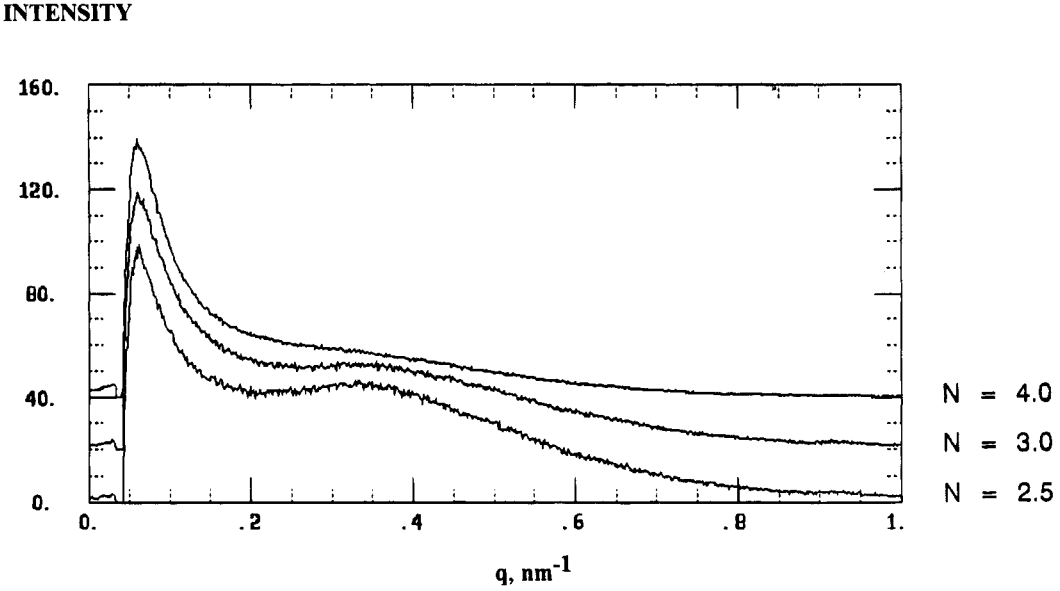

Figure 3. SAXS patterns (intensity vs q, nm^{-1}) of polyurethanes D, I, and J (reading from the bottom curve upward) of Table 1, of composition CHDI:PTMO:BD = N:1:(N − 1); the PTMO has a nominal M_n of 2000. The N value is indicated to the right of each plot. Successive plots are offset by an upward baseline shift.

for this purpose; the results are reported in Table 6 as μ_{HP} and ϱ_{HP}, the mass and electron densities calculated for the hard-segment microphase. (In every case, the iteration converged to within 0.000 01 for ϱ_{HP} in less than six iterations.)

The computed values of μ_{HP} or ϱ_{HP} are remarkably consistent for results of this kind, particularly if one excludes the four samples I, J, L, and M, having the common property that the ratio of moles of BD to moles of PTMO is 2.0 or greater, i.e., for which the hard segments must include species larger than the simple moiety CHDI–BD–CHDI. With these four samples excluded, the calculated values of μ_{HP} range from 1.35_2 to 1.36_3 g/cm^3, while the calculated ϱ_{HP} values range from 0.69_5 to 0.70_4 mol e/cm^3. This remarkable consistency very much suggests that the calculated μ_{HP} and ϱ_{HP} values represent the mass and electron densities of a pure hard-segment phase consisting primarily of –CHDI–BD–CHDI–. (It is recognized that, due to the method of synthesis, there will be a distribution in the molar composition of hard-segment species, with the stoichiometry reflecting the average composition of the various hard-segment species.) The four excluded samples exhibit lower hard-segment mass and electron densities resulting, presumably, from the fact that their hard-segment stoichiometry requires a high fraction of species as large as CHDI–BD–CHDI–BD–CHDI, in addition to the species CHDI–BD–CHDI, in the hard-segment microphase. The inclusion of significant amounts of the larger species results in a less efficiently packed hard-segment microphase.

To further display these results, a second calculation was performed, obtaining calculated electron density variance values employing eq 10 with a value of 1.35_7 g/cm^3, the average of the nine nonexcluded iteration results, for μ_H. In effect, we are now using the pure hard-segment density values established above to calculate variance values $\langle \Delta\varrho_e^2 \rangle_P$ for the pure microphase,

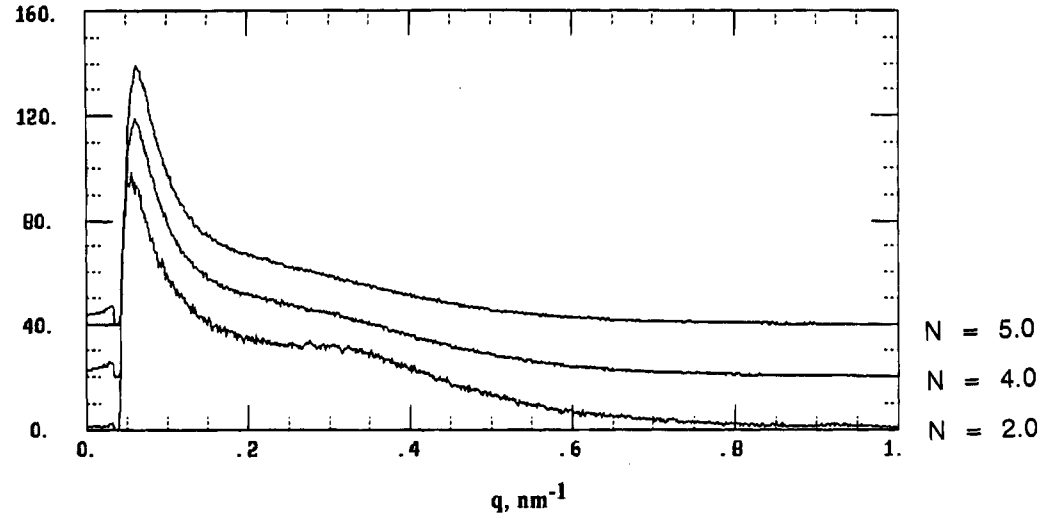

Figure 4. SAXS patterns (intensity vs q, nm^{-1}) of polyurethanes K, L, and M (reading from the bottom curve upward) of Table 1, of composition CHDI:PTMO:BD = N:1:(N − 1); the PTMO has a nominal M_n of 2900. The N value is indicated to the right of each plot. Successive plots are offset by an upward baseline shift.

Table 6. Results of Iterative Calculation To Obtain Hard-Segment Phase Densities from Experimental Electron Density Variance Values

sample	data for iteration: expt variance $\langle\Delta\varrho_e^2\rangle \times 10^3$,[a] (mol e/cm^3)^2	iterative calculation results: estimated hard segment: vol fract ϕ_{HP}, (v/v)	mass density μ_{HP}, g/cm^3	electron density ϱ_{HP}, mol e/cm^3	inhomogeneity lengths, nm: total L_C	hard L_H	soft L_S	electron density variance calculation[d]: calcd variance $\langle\Delta\varrho_e^2\rangle_P \times 10^3$,[b] (mol e/cm^3)^2	expt/calcd variance ratio
A	3.18	0.152	1.358	0.703	2.25	2.66	14.8	3.15	1.01
B	3.29	0.157	1.361	0.704	2.62	3.11	16.6	3.21	1.02
C	3.31	0.163	1.359	0.702	2.59	3.10	15.9	3.27	1.01
D	3.22	0.169	1.352	0.698	2.64	3.17	15.7	3.32	0.97
E	3.49	0.181	1.357	0.700	2.72	3.32	15.0	3.49	1.00
F	3.64	0.186	1.361	0.701	2.85	3.51	15.3	3.54	1.03
G	3.41	0.185	1.354	0.697	2.94	3.60	16.0	3.48	0.98
H	3.42	0.190	1.352	0.695	3.06	3.77	16.1	3.53	0.97
I[c]	3.53[c]	0.210[c]	1.338[c]	0.692[c]	2.58	3.25	12.4	3.98[c]	0.89[c]
J[c]	3.95[c]	0.270[c]	1.327[c]	0.688[c]	3.13	4.26	11.8	4.81[c]	0.82[c]
K	2.14	0.100	1.363	0.701	2.61	2.89	26.2	2.06	1.04
L[c]	3.52[c]	0.198[c]	1.341[c]	0.695[c]	3.43	4.26	17.5	3.89[c]	0.90[c]
M[c]	3.44[c]	0.243[c]	1.316[c]	0.683[c]	3.69	4.84	15.6	4.52[c]	0.76[c]

[a] Experimental electron density variance. [b] Calculated electron density variance. [c] Polymers in which the ratio mol of BD/mol of PTMO is 2.0 or greater. [d] Using μ_H = 1.357 g/cm^3 from the iterative calculation, excluding samples marked with *c*.

sharp boundary model for comparison with the experimental variances $\langle\Delta\varrho_e^2\rangle'$. These calculated variances are shown in column 6 of Table 6, while the ratio of experimental to calculated variance values is shown in column 7. For the nine elastomers having BD/PTMO less than 2.0, this ratio ranges from 0.97 to 1.04, equivalent to 1.00 within experimental error, indicating a near perfect level of microphase separation, assuming a microstructure having μ_{HP} and μ_{SP} values of 1.36 and 0.985 g/cm^3, respectively. For the remaining four elastomers, having BD/PTMO greater than or equal to 2.0, the ratio ranges from 0.76 to 0.89; for such ratios we must conclude that either (a) some segmental mixing has occurred, altering either μ_H, μ_S, or both, or (b) there is NO segmental mixing between the microphases, but the actual μ_H value is less than 1.36 g/cm^3. Note that one cannot assume a priori that μ_H will be independent of the hard-segment length.

Others have used such a ratio of experimental to ideal variance values as a measure of the degree of the overall microphase separation. To place these results in perspective, it is instructive to compare the present results to those in the literature. The corresponding ratios reported by Koberstein and Stein,[23] for polyurethanes of MDI/BD[35] or TDI/EG,[35] are in the range 0.31−0.41, while the ratios reported by Leung and Koberstein[29] for MDI/BD polyurethanes range from 0.17 to 0.37. Van Bogart, Gibson, and Cooper[36] report variance ratios ranging from 0.35 to 0.51 for polyurethanes containing MDI/BD. Viewed with respect to these earlier results, all of the present variance ratios, ranging from 0.76 to 1.04, are seen as quite high, pointing to the conclusion that the CHDI/BD class of urethane elastomers achieves, in general, much better microphase separation than the MDI/BD or TDI/EG classes previously studied.

Microphase Separation As Studied by SAXS: Effect of Temperature. The changes in microphase separation with temperature, in both heating and cooling, are shown in Figures 5 and 6 for urethanes of compositions D and L as listed in Table 1. The most remarkable aspect of these SAXS patterns is that, on a qualitative basis, there is relatively little change in the patterns between 30 and 275 °C. Compare these patterns, for instance, with the recent data of Chu and

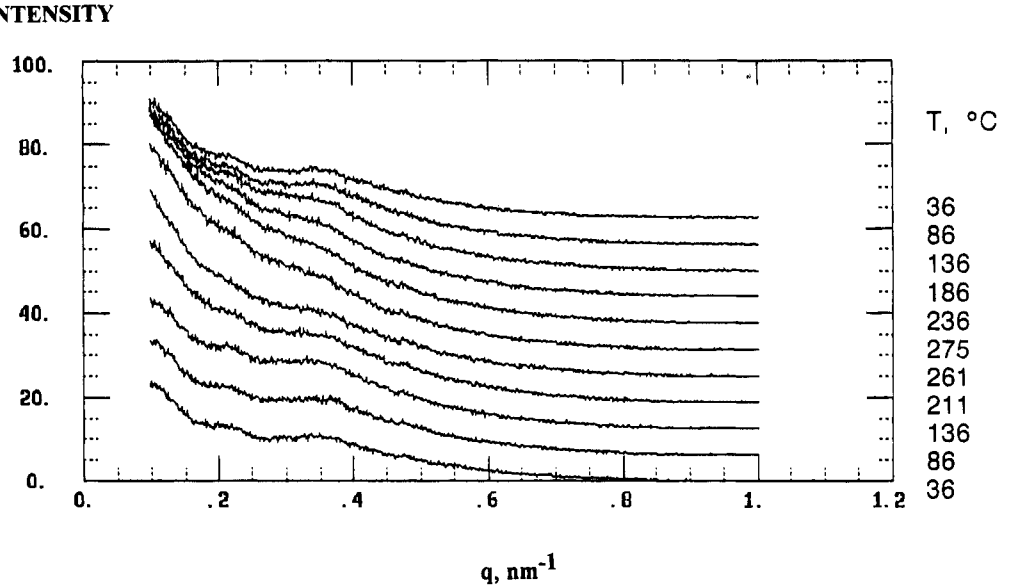

Figure 5. SAXS heating experiment (intensity vs q, nm^{-1}) of polyurethane D from Table 1. Temperatures are indicated along the right vertical axis. Scans at intermediate temperatures are omitted, and successive plots are offset by an upward baseline shift.

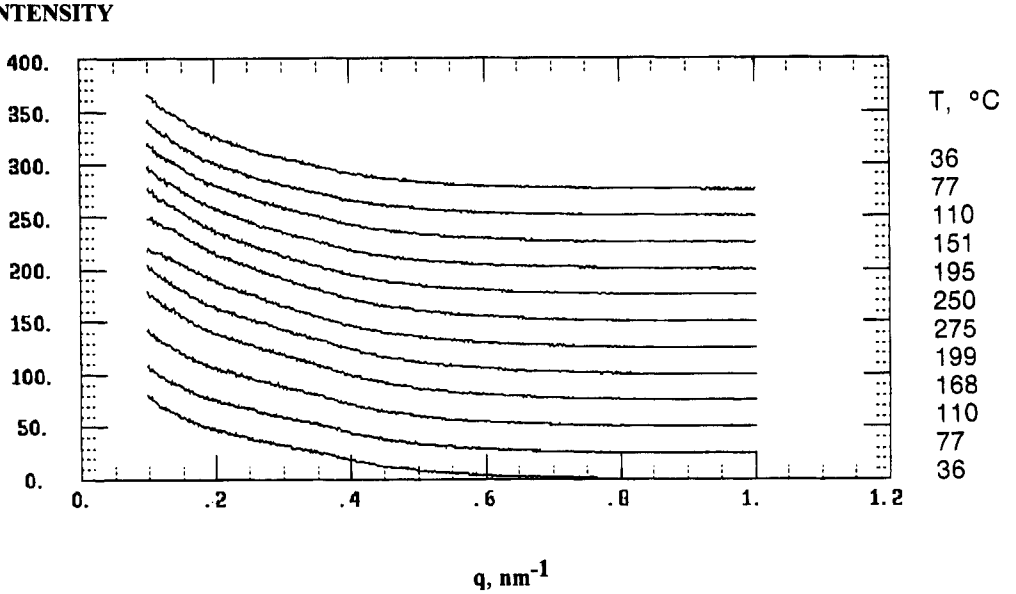

Figure 6. SAXS heating experiment (intensity vs q, nm^{-1}) of polyurethane L from Table 1. Scans at intermediate temperatures are omitted, and successive plots are offset by an upward baseline shift.

co-workers,[6,8] where, for urethanes having MDI–BD hard segments, the SAXS pattern essentially disappeared at 220 °C, at which temperature the homogeneous melt is stable. The present SAXS data are direct evidence of the persistence of microphase separation in the present CHDI/BD urethanes to quite high temperatures, accounting for the quite high softening temperatures reported by Byrne et al.[19] for this class of elastomers.

For a more quantitative look at the temperature effects on the microstructure of the present urethanes, the relative values of the electron density variance have been calculated, using the Porod invariant method, from the SAXS data of Figures 5 and 6, and are shown in Figures 7 and 8. Again, the most remarkable feature is the persistence of strong microphase separation, as evidenced by high electron density variance values, to 275 °C. This is in marked contrast to analogous data for MDI/BD polyurethanes,[8,33] showing a rapid drop in the variance value with increasing temperature in the range 160–200 °C. The persistence in the strength of the variance curve with temperature for the CHDI/BD polyurethanes is in agreement with the excellent high-temperature mechanical properties previously reported[19] for CHDI/BD polyurethanes.

Both polymers D and L show some irreversibility in their variance vs temperature curves (Figures 7 and 8), but of a markedly different nature. Comparing the compositions in Table 1, the two polymers differ mostly in the lengths of their average hard and soft segments. For polymer D, the average hard-segment sequence is 2.5 CHDI and 1.5 BD residues; for polymer L, it is 4.0 CHDI and 3.0 BD residues. Polymer L also has the longer soft segment of the two (M_n = 2862 vs 2033); the two effects compensate so that there is only a comparatively small difference in the weight fraction hard segment, 0.239 vs 0.206.

For polymer D, with the shorter hard and soft segments of the two, the variance behavior is quite reversible in the range 36–185 °C but becomes pro-

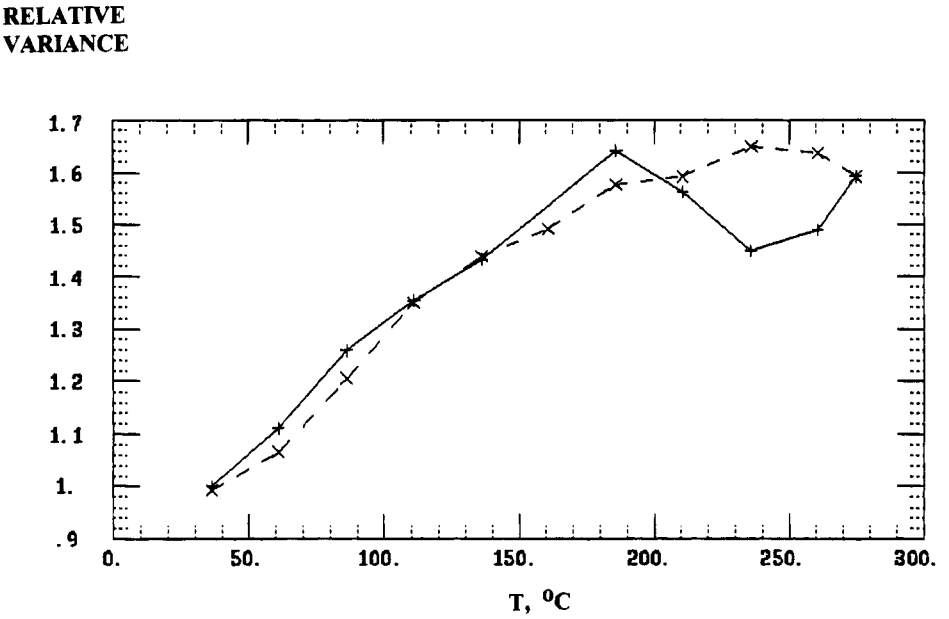

Figure 7. Relative values of electron density variance for the SAXS heating experiment of Figure 7, polyurethane D. Solid line (+): ascending temperatures. Dashed line (×): descending temperatures.

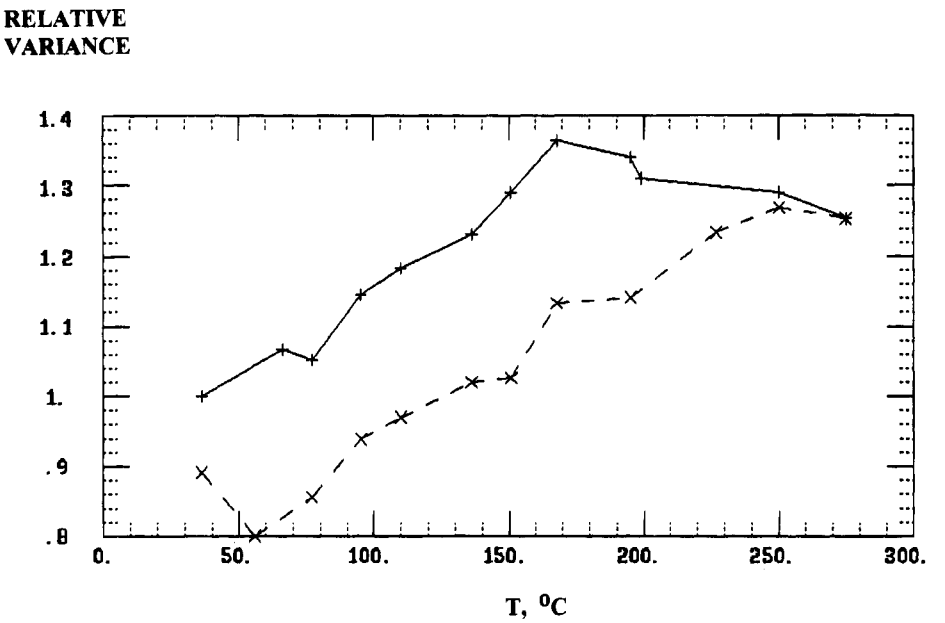

Figure 8. Relative values of electron density variance for the SAXS heating experiment of Figure 8, polyurethane L. Solid line (+): ascending temperatures. Dashed line (×): descending temperatures.

nouncedly irreversible in the 185–275 °C range. This irreversibility probably results from a hard-segment transition, since the 185 °C onset of this hysteresis region coincides with that of a hard-segment transition previously reported from DSC experiments.[19] Note, however, that the detailed shape of the SAXS curve at 36 °C is changed (see Figure 5) in the process of the heating experiment, particularly in the range below $q = 0.3$ nm^{-1}. This indicates that certain details of the microstructure have changed in the heating and cooling process, although the invariant value has not. The changes have affected only the lower q region of the SAXS curve, while the invariant is much more sensitive to the higher q region than the lower q region.

The response of polymer D to the temperature cycle may also be illustrated quantitatively, by reference to the starting and ending values of both the invariant and the inhomogeneity length. At the outset, the invariant value, on a relative basis, is 0.89_4, while the ending value is 0.88_8, both measured at 36 °C. The difference of less than 1% is insignificant and may be attributed to experimental error. On the other hand, the inhomogeneity length is found to increase by over 7% between the start and end. Thus, it is seen that the overall change in microstructure involves little change in the electron density variance, coupled with a 7% increase in the microstructure size parameter. It is apparent that the scattering entities have become more extended in size—possibly improving their order by lateral accretion—but have not changed in terms of the degree of microphase separation.

The variance behavior (Figure 8) of polymer L, having the longer hard and soft segments, is quite different. In this case, the variance falls off continuously in the 195–275 °C range with rising temperature, but not precipitously: microphase separation is still present at 275 °C. As the temperature is lowered, however, the variance does not follow the ascending temperature

curve at all, staying well below that curve throughout the cooling cycle to 36 °C. The irreversibility in the polymer L case is attributed to nonequilibrium behavior, possibly associated with kinetic effects. Presumably some segmental mixing is occurring with rising temperature above 195 °C but is not recovered in the decreasing temperature curve. Either the original microstructure was not in the equilibrium state or slow kinetics for the process of re-forming the microstructure cause the irreversibility. In terms of numerical parameters, polymer L showed an 11% decrease in the electron density variance, while the inhomogeneity length increased 6% in the heating cycle.

Discussion

The wide-angle X-ray diffraction data indicate that a paracrystalline hard-segment phase is formed at the 100 °C synthesis temperature in these elastomers. When the cured elastomers are heated above the synthesis temperature, some hard-segment reorganization takes place as indicated by the DSC thermal transition at 185 °C. Hard-segment crystallization is difficult; only under such severe conditions as heating for 16 h at 150–160 °C are crystallites showing multiple sharp crystalline peaks observed.[19] The above observations indicate that although the neighboring CHDI/BD residues in the hard-segment microphase have quite strong attractions for each other, as suggested by the model compound studies of Jasinski,[20] these attractions can be achieved to a great extent by a structure lacking long-range crystalline order. Thus the repeating units can pack with sufficient proximity to drop into energy wells, resulting in a paracrystalline structure characterized by a single sharpened diffraction peak at 0.43–0.44 nm. The strength of these local interactions of like hard-segment residues is also indicated by the fact that (unlike most other segmented urethanes) the CHDI/BD segmented urethanes do not readily dissolve in solvents. The energy benefit of having like hard-segment neighbors outweighs the entropy benefit of mixing with either soft-segment species or with solvent.

The microstructure, as revealed by SAXS, is characterized by sharp interfacial boundaries and high degrees of segmental segregation, considerably higher than that previously observed for other classes of polyurethanes. The polymer separates into effectively pure microphases for the lower molar content of the hard segment, while a higher hard-segment content (BD/PTMO ratio 2.0 and above) results in some segmental mixing, but less than for other classes of polyurethanes. In this discussion it is recognized that there will be a distribution in the length of hard-segment species. Thus while stoichiometry will determine the average length of a hard-segment sequence, there will be an appreciable content of hard segments with lengths somewhat above and below that average value.[34] Thus a polymer such as K in Table 1, whose hard-segment stoichiometry corresponds to the hard-segment dimer –CHDI–BD–CHDI–, will nonetheless contain appreciable amounts of both the monomeric hard segment –CHDI– and the trimeric hard segment –CHDI–BD–CHDI–BD–CHDI–, each terminated at both ends by the start of a soft segment. Information as to the actual hard-segment length distribution for these polymers is not, however, readily available.

Koberstein and co-authors[23,33] have discussed the morphology of hard-segment microphases in terms of the distribution of lengths of hard-segment species in the hard-segment microdomain. For the classes of hard segments they studied (abbreviated MDI/BD and of TDI/EG) they found it necessary to modify the earlier model of Bonart,[3] depicting parallel packing of the hard-segment species, by proposing the folding or coiling of hard segments within the hard-segment microdomains. This allows the longer hard-segment sequences to coexist with shorter sequences in a hard-segment microdomain by folding itself back into the microdomain rather than dangling into the soft-segment microdomain. Koberstein and Stein[23] find support for this proposal in terms of the values of microdomain thickness and boundary layer thickness derived from SAXS data and in terms of the melting points of hard-segment model compounds.

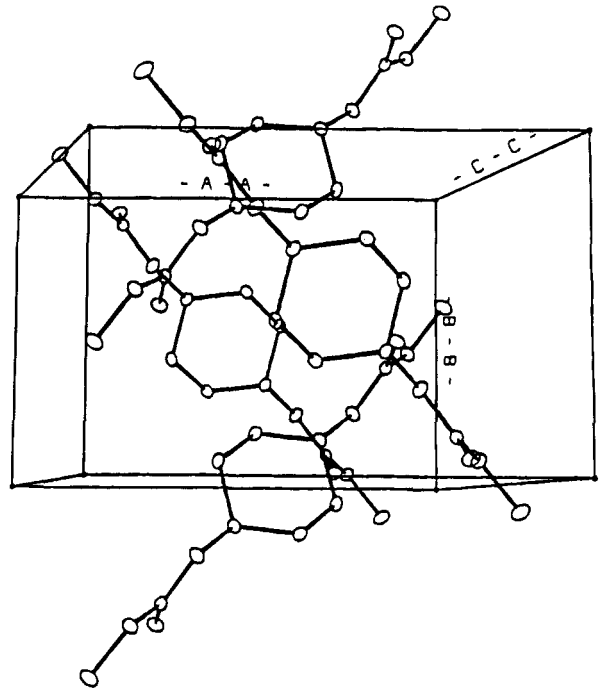

Figure 9. Packing diagram of the model compound $C_{10}H_{18}N_2O_4$, CHDI end-capped with methanol, based on ref 20; space group $P2_1/c$. Lattice parameters: a = 1.0563 nm, b = 0.7265 nm, c = 0.8375 nm; β = 106.87°.

Koberstein bases his discussion on a lamellar microstructure, which may or may not be present in the CHDI/BD polyurethanes. For instance, in model compound studies[20] for these hard segments, a structure of space group $P2_1/c$ occurs, in which the chains do not pack in the usual parallel fashion common to polymeric crystals. Instead, the chains pack in a "herringbone" fashion, as shown in Figure 9, with all of the chains in the a–b plane but with half of them at an angle of (roughly) 45° with the b axis, while the other half make an angle of (roughly) –45°. Thus the two sets of chains cross each other at (approximately) a 90° angle rather than in the parallel fashion that Koberstein assumes for lamellar microstructures.

In Figure 10, a possible structure for a CHDI/BD hard-segment microdomain analogous to that of the $P2_1/c$ model compound structure is shown schematically, with the species –CHDI–BD–CHDI– represented as a dumbbell. In each dumbbell the cyclohexyl moieties are represented as spheres, and the urethane/aliphatic residue forms the connecting bar between the spheres. Successive dumbbells add to the stack offset alternately to the left and the right of a crystal axis, resulting in a columnar morphology, rather than the usual lamellar

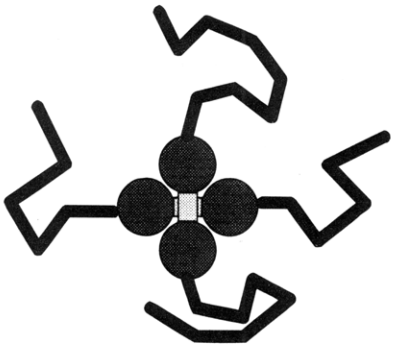

Figure 10. Proposed packing of −CHDI−BD−CHDI− hard-segment dimers in analogy to the model compound structure of Figure 9. The spheres represent the cyclohexyl residues; the connecting bars represent the urethane/aliphatic linkages. The broken lines emanating from the dumbbells represent the soft segments.

structure. Thus the soft segments, shown as solid lines in Figure 10, would splay out in all directions from the central column of the hard-segment microphase, connecting with adjacent columnar structures to form an elastomeric network.

The data presently available are not sufficient to verify or contradict the Figure 10 structure for the hard-segment microphases in the elastomers studied. However, it is important to note that the possibility of such structures implies that one may not need to presume a lamellar microstructure. A columnar structure, elongated in the (002) direction perpendicular to both of the crossed chains of Figure 10 but limited in size within the plane common to the crossed chains, would be a more appropriate microstructure to that particular hard-segment structure. Furthermore, the basic difference between lamellar structures and columnar structures means that the arguments of Koberstein et al.[23,33] regarding folding of longer hard segments may not apply to urethane elastomers of the CHDI class.

The Figure 10 structure has only one-dimensional order, repeating in the c direction, the direction normal to the paper of the figure and perpendicular to the rods of both dumbbells. It is in this c direction that successive layers of hard segment stack; the structure does not repeat within the plane of the layers. Thus the only diffraction spacings one would expect to observe would be the repeat distance between successive stacks of chains, analogous to the (002) distance of the model compound, and its orders (if any). This predicted repeat value is $d_{002} = c/2 = 0.4288$ nm, in reasonably good agreement with the paracrystalline spacing of 0.46 nm.

It is recognized that an actual polymer will contain a distribution of hard-segment lengths. Thus one must consider structures of mixed hard-segment lengths as well as structures comprising hard segments all of the same length. One must also allow the possibility that the equilibrium hard-segment structure (in terms of whether the chains are parallel or crossed) could well vary from one hard-segment length to the next. Fractionation of hard segments into microdomains each of a single hard-segment length could well prove to be a very slow process; thus structures of mixed hard-segment lengths could be favored kinetically. In this regard, the fact that the interface thicknesses σ are found to be effectively zero suggests strongly that chain folding must occur for the longer hard-segment species.

Consider the structure of Figure 10, and suppose that the next hard-segment species to add on top is a longer hard-segment species, having more than two diisocyanate residues. Suppose the third diisocyanate residue dangles into the surrounding soft-segment material: the dangling hard-segment material would then contribute its higher electron density to an interface zone of intermediate density. Since such an interface zone is not evident in the SAXS data, one concludes that the longer hard-segment species do not dangle into the soft-segment material; instead, they fold back into the hard-segment structure at a higher stacking position.

While it is recognized that segretation of hard-segment species by hard-segment length is disfavored kinetically, it may well be favored thermodynamically, providing an impetus for reorganization of the microstructure during annealing at elevated temperatures, e.g., above 200 °C. Further studies of a variety of model compounds would be required to elucidate such effects.

Acknowledgment. This research was sponsored by the U.S. Army Research Laboratory, the U.S. Army Research Office (DAAH0494G0053), and the Department of Energy (No. DEFG086ER45237A010). The authors thank the SUNY beamline at the National Synchrotron Light Source, Brookhaven National Laboratory, and Mr. Alex Chin and Dr. Janice Dieter, formerly of the Army Research Laboratory, for their invaluable assistance.

References and Notes

(1) Dieter, J. W.; Byrne, C. A. *Polym. Eng. Sci.* **1987**, *27*, 673.
(2) Bonart, R. *J. Macromol. Sci., Phys.* **1968**, *B2*, 115.
(3) Bonart, R.; Morbitzer, L.; Hentze, G. *J. Macromol. Sci., Phys.* **1969**, *B3*, 337.
(4) Bonart, R.; Muller, E. H. *J. Macromol. Sci., Phys.* **1974**, *B10*, 177, 345.
(5) Bonart, R.; Morbitzer, L.; Muller, E. H. *J. Macromol. Sci., Phys.* **1974**, *B9*, 447.
(6) Chu, B.; Gao, T.; Li, Y.; Wang, J.; Desper, C. R.; Byrne, C. A. *Macromolecules* **1992**, *25*, 5724.
(7) Porod, G. *Kolloid Z.* **1951**, *124*, 83; **1952**, *125*, 51, 109. Guinier, A.; Fournet, G. *Small Angle Scattering of X-rays*; Wiley: New York, 1955; pp 157−160. Van Bogart, J. W. C.; Lilaonitkul, A.; Cooper, S. L. *Adv. Chem. Ser.* **1979**, *176*, 3. Vonk, C. G. In *Small Angle X-ray Scattering*; Glatter, O., Kratky, O., Eds.; Academic Press: New York, 1982; pp 433−466. Desper, C. R.; Schneider, N. S. In *Polymer Alloys III*; Klempner, D., Frisch, K. C., Eds.; Plenum Publications: New York, 1983; p 233.
(8) Li, Y.; Gao, T.; Liu, J.; Linliu, K.; Desper, C. R.; Chu, B. *Macromolecules* **1992**, *25*, 7365.
(9) Schneider, N. S.; Desper, C. R.; Illinger, J. L.; King, A. O.; Barr, D. *J. Macromol. Sci., Phys.* **1975**, *B11*, 527.
(10) Wilkes, C. E.; Yusek, C. S. *J. Macromol. Sci., Phys.* **1973**, *B7*, 157.
(11) Blackwell, J.; Lee, C. D. *J. Polym. Sci., Polym. Phys. Ed.* **1984**, *22*, 759.
(12) Born, L.; Crone, J.; Hespe, H.; Muller, E. H.; Wolf, K. H. *J. Polym. Sci., Polym. Phys. Ed.* **1984**, *22*, 163.
(13) Christenson, C. P.; Harthcock, M. A.; Meadows, M. D.; Spell, H. L.; Howard, W. L.; Creswick, M. W.; Guerra, R. E.; Turner, R. B. *J. Polym. Sci., Polym. Phys. Ed.* **1986**, *24*, 1401.
(14) Clough, S. B.; Schneider, N. S. *J. Macromol. Sci., Phys.* **1968**, *B2*, 553.
(15) Harrell, L. L., Jr. *Macromolecules* **1969**, *2*, 607.
(16) Allegrezza, A. E., Jr.; Seymour, R. W.; Ng, H. N.; Cooper, S. L. *Polymer* **1974**, *15*, 433.
(17) Tao, H.-J.; Fan, C. F.; MacKnight, W. J.; Hsu, S. L. *Macromolecules* **1994**, *27*, 1720.
(18) Siegmann, A.; Cohen, D.; Narkis, M. *Polym. Eng. Sci.* **1987**, *27*, 1187.
(19) Byrne, C. A.; Mead, J.; Desper, C. R. *Adv. Urethane Sci. Technol.* **1992**, *11*, 68.
(20) Jasinski, J. P.; Desper, C. R.; Zentner, B. A.; Byrne, C. A.; Butcher, R. J. *Acta Crystallogr.* **1988**, *C44*, 1137.
(21) Chu, B.; Wu, D.; Wu, C. *Rev. Sci. Instrum.* **1987**, *58*, 1158.
(22) Kratky, O. *Z. Anal. Chem.* **1964**, *201*, 161.

(23) Koberstein, J. T.; Stein, R. S. *J. Polym. Sci., Polym. Phys. Ed.* **1983**, *21*, 1439.
(24) Kratky, O.; Pilz, I.; Schmitz, P. J. *J. Colloid Interface Sci.* **1966**, *21*, 24.
(25) Russell, T. P.; Lin, J. S.; Spooner, S.; Wignall, G. D. *J. Appl. Crystallogr.* **1988**, *21*, 629.
(26) Ruland, W. *J. Appl. Crystallogr.* **1971**, *4*, 70.
(27) Koberstein, J. T.; Morra, B.; Stein, R. S. *J. Appl. Crystallogr.* **1980**, *13*, 34.
(28) Roe, R.-J. *J. Appl. Crystallogr.* **1982**, *15*, 182.
(29) Leung, L. M.; Koberstein, J. T. *J. Polym. Sci., Polym. Phys. Ed.* **1985**, *23*, 1883.
(30) Kratky, O.; Porod, G.; Skala, Z. *Acta Phys. Aust.* **1960**, *13*, 76.
(31) Shaffer, L. B.; Hendricks, R. W. ORNL-TM-4278, Oak Ridge National Laboratory, Oak Ridge, TN, 1973.
(32) Ruland, W. *Colloid Polym. Sci.* **1977**, *255*, 417.
(33) Koberstein, J. T.; Russell, T. P. *Macromolecules* **1986**, *19*, 714.
(34) Peebles, L. H. *Macromolecules* **1976**, *9*, 58.
(35) Nomenclature: MDI is 4,4′-diphenylmethanediisocyanate; TDI is (in this instance) an 80/20 mixture of 2,4- and 2,6-toluenediisocyanate; BD is 1,4-butanediol; EG is ethylene glycol.
(36) Van Bogart, J. W. C.; Gibson, P. E.; Cooper, S. L. *J. Polym. Sci., Polym. Phys. Ed.* **1983**, *21*, 65.

MA9461456